Clays Clay Miner., Vol. 70, No. 6:865–881, 2022
https://doi.org/10.1007/s42860-023-00228-6

ORIGINAL PAPER

Preparation and Properties of Sepiolite-Based 3D Flame-Retardant Aerogel

Yelei Hu · Tong Xu · Hong Xu · Yi Zhong · Linping Zhang · Bijia Wang · Xiaofeng Sui · Xueling Feng · Zhiping Mao

Accepted: 27 March 2023 / Published online: 5 May 2023

Abstract Sepiolite-based composites have great potential for application as flame-retardant and thermal-insulation material but their application and development are limited by poor mechanical properties. The objective of the present study was to combine polyvinyl alcohol (PVA) and 3-aminopropyltriethoxysilane (KH-550) with sepiolite (Sep) to improve its aerogel strength. A universal testing machine, thermogravimetry, and microcalorimetry were used to investigate the mechanical properties, thermal-stability, and flame-retardant properties, respectively, of aerogels. The results indicated that KH-550 can enhance effectively the mechanical properties and flame retardancy of aerogels. The compressive modulus of PVA/Sep vs KH-550/PVA/Sep aerogel was 209.28 vs. 474.43 kPa, the LOI index changed from 26.4 to 30.4%. The porosity of the aerogels was > 96% and the density was < 0.05 g/cm^3. The thermal conductivity remained at between 0.0340 and 0.0390 W/(m·K), and the aerogel could recover to > 85% after a 50% compressive deformation. These data indicated that Sep-based aerogel would act as a flame retardant and a thermal insulating material with excellent mechanical properties.

Keywords Compressive modulus · Flame retardancy · Freeze-drying · Mechanical property · PVA/Sep aerogel

Introduction

Aerogel is an ultra-low-density material with small pore size, high porosity, rich pore structure, and

Y. Hu · H. Xu · Y. Zhong · L. Zhang · B. Wang · X. Sui · X. Feng · Z. Mao (✉)
Key Lab of Science and Technology of Eco-Textile, Ministry of Education, College of Chemistry and Chemical Engineering, Donghua University, Shanghai 201620, China
e-mail: zhpmao@dhu.edu.cn

T. Xu
Shanghai Technical Institute of Electronics & Information, Sino-German Engineering College, No. 3098, Wahong Highway, Fengxian District, Shanghai, China

H. Xu · Y. Zhong · L. Zhang · B. Wang · X. Sui · X. Feng · Z. Mao
Shanghai Belt and Road Joint Laboratory of Textile Intelligent Manufacturing, Innovation Center for Textile Science and Technology, Donghua University, Shanghai 201620, China

H. Xu · Y. Zhong · L. Zhang · B. Wang · X. Sui · X. Feng · Z. Mao
National Innovation Center of Advanced Dyeing & Finishing Technology, Shandong Zhongkang Guochuang Research Institute of Advanced Dyeing & Finishing Technology Co. Ltd, Taian City 271000, Shandong Province, China

a large specific surface area and which can be used in a variety of applications such as heat insulation, industrial catalysis, and supercapacitors. The first use of a supercritical drying technique to synthesize aerogel was by Kistler (1931). Because of the unique nanoskeletal network of silica-aerogel, the material has a very wide range of applications. The main disadvantage of silica-based aerogel materials is that they are very fragile, produce very small fragments that are harmful to human health, and are generally produced through a high-cost supercritical drying process. In recent years, a number of studies (Chen et al., 2013; Wang et al., 2022) have demonstrated that flexible material with porous structures can be used to replace silica-based aerogels. Clay offers promise in this regard (Hostler et al., 2009). Due to the charged basal and edge surfaces of clay crystals, a unique 'card house' structure could be formed, which is very favorable for the building of aerogel materials. Clay-based aerogels also offer promise because of their low cost and ready availability (Hostler et al., 2009). Pure clay-based aerogel is very fragile, however, and requires the addition of a polymer as a reinforcement to improve its mechanical properties. For example, biodegradable foams were prepared by: adding pectin to Na^+-montmorillonite (Na^+-Mnt) as a substrate and multivalent cations as cross-linkers (the cross-linker is $CaCl_2$; Ca^{2+} can promote the formation of crosslinking networks in pectin) (Chen et al., 2013); aerogels with good mechanical properties for packaging materials were prepared by adding natural rubber to Na^+-Mnt and S_2Cl_2 as a cross-linker (Pojanavaraphan et al., 2011); aerogel materials with photothermal-conversion and energy-storage capabilities were prepared by adding pectin to palygorskite (Plg) and Ca^{2+} initiated cross-linking (Ca^{2+} is used to initiate crosslinking, resulting in obvious crosslinking of pectin in the system) (Wang et al., 2022); the addition of cellulose nanofibers to Sep and cross-linking with glutaraldehyde to prepare aerogels with good heat-shielding and flame-retardant properties (Gupta et al., 2019). Among several types of clay, Sep has received much attention for its unique structure.

Sepiolite ($Mg_8(OH)_4Si_{12}O_{30}{\cdot}nH_2O$, Sep) is a silicate mineral with a large specific surface area (up to 900 m^2/g) and a significant porosity (Liu et al., 2018; Lv et al., 2017). It is fibrous with lengths of ~0.20–4.00 μm, widths of ~10–30 nm, and thicknesses of ~5–10 nm. The shape allows penetration by polymeric chains into the internal space channels of Sep (Khan et al., 2022). The crystalline structure of Sep is made up of continuous tetrahedral sheets of silicon-oxygen. Each silicon-oxygen tetrahedron shares two angular vertices and is connected to three adjacent tetrahedra. Reactive oxygen species in the tetrahedron are periodically inverted along the *b* axis, forming open channels parallel to the chain of fixed wells and containing zeolite water (Rytwo et al., 1998). At the edge of the octahedron, two water molecules bind to the magnesium ions and participate in octahedral coordination. Sep has been used widely in agriculture, geology (oil drilling mud), lithium ion batteries, adsorption carriers, and cement-based gypsum preparation, etc. (Fernandez-Barranco et al., 2016; Konuklu & Ersoy, 2016; Shen et al., 2017). Compared with other clays (such as montmorillonite and palygorskite), Sep has zeolite water channels and pores throughout the structure (the zeolite water structure of sepiolite runs through the entire structure, while the zeolite water of Plg only exists in the relatively wide position of inert oxygen). The micromorphology has a hollow brick fiber structure which is similar to carbon fiber, large aspect ratio, low shrinkage rate, good dimensional stability, and a low thermal expansion coefficient, showing excellent mechanical and thermal shielding properties. At the same time, due to the discontinuity of the outer silicon sheet of Sep, its surface is covered with free silanol groups, which can react with organosilane coupling agents to form stable covalent bonds (Li et al., 2013). Large reserves of Sep are found in China; they are low cost, non-toxic, and the mineral is harmless to humans. Sepiolite is recognized as the most adsorptive clay and has good thermal stability and corrosion resistance; it has been used in many applications, and offers significant promise in environmental protection, building materials, etc. (Alkan et al., 2005). The one-dimensional fibrous structure of Sep is preferred for the assembly of aerogel materials, as opposed to the two-dimensional layered structure of montmorillonite or the three-dimensional rod-like structure of palygorskite.

Conventional thermal insulation and flame-retardant materials are made of mineral wool, expanded perlite, foamed polystyrene, foamed polyurethane, etc. Compared with these materials, Sep is non-toxic and harmless, and its aerogels are significantly better than conventional thermal insulation

https://doi.org/10.1007/s42860-023-00228-6 Published online by Cambridge University Press

materials in terms of porosity and density. In addition, the preparation process for Sep-based aerogel is simple and does not need extra adhesive that is harmful to humans; nor will it cause serious pollution during the production process. Few studies exist on the use of Sep in the preparation of aerogels with thermal insulation and flame-retardant properties.

The clay-based aerogel prepared by Sep with low density (<0.1 g/cm^3) and high porosity (85–95% porosity) is very fragile (Johnson et al., 2009; Pojanavaraphan et al., 2010). Added polymer is needed as a reinforcement to improve the mechanical and other specific properties of the aerogels such as hydrophobic and oilphobic properties, ultra-high and ultra-low temperature resistance properties and infrared shielding performance (Madyan & Fan, 2019; Salehi et al., 2021). Polyvinyl alcohol (PVA) is a suitable candidate in the production of clay aerogel composites due to its relatively low cost, non-toxicity, good mechanical properties, biocompatibility, solubility in water, and strong attraction to clays. Due to its ideal hydrogen bonding, i.e. the hydrogen on the polymer is perfectly spaced to match the oxygen in the lattice of the Sep, PVA/Sep aerogel offers a significant mechanical enhancement (Madyan et al., 2016).

The present study aimed to prepare PVA/Sep composites by freeze-drying. The best-performing composite was selected from among a range of options in terms of the optimal ratio, to obtain Sep-based aerogel with good compression resilience, low thermal conductivity, excellent thermal insulation performance, and flame-retardant performance.

Experimental

Materials

Polyvinyl alcohol (PVA, AR, 87–89% hydrolyzed) was purchased from Macklin (Shanghai, China). Sepiolite (Sep, Purity: 99%) was purchased from Sigma-Aldrich, (Newark, New Jersey, USA). Hydrochloric acid (AR, 36–38%) was purchased from Guoyao, Shanghai, China. The crosslinking agent (KH-550, $(C_2H_5O)_3$-Si $(CH_2)_3NH_2$, AR, M.W 221) was purchased from Aladdin (Shanghai, China). All materials were used as received, without purification.

Preparation of Aerogel Samples

Sep and a certain volume of aqueous solution with adjusted pH were placed in a 100 mL beaker and the beaker was placed under the high-speed disperser (IKA T25, Suzhou Sainz Instrument Co., Ltd., Suzhou, China) at 12,000 rpm (400π ω/s) for 30 min to obtain a 3 wt.% Sep suspension. 3 g of PVA was dissolved in water at 90℃ by mechanical stirring for 4 h to obtain a 3 wt.% PVA solution. Then PVA solution (or PVA solution and cross-linker KH-550) was added to the Sep suspension at 80℃ and stirred for 2 h to obtain a uniform mixture. The mixture was poured into Teflon molds placed on a copper rod in contact with a liquid nitrogen bath. The mixture was frozen while the liquid nitrogen level was kept up to the height of the copper rod, then freeze-dried at –55℃ and 15 Pa for 48 h in a freeze dryer (Labconco FD5-3, Kansas City, Missouri, USA). The dried samples were placed in an oven at 110 °C for 30 min in order to promote cross-linking (Cheng et al., 2018; Liu et al., 2021) (Fig. 7a compares the stress–strain curves of P3S5K5 heated in a 110°C oven for 30 min with those without heat treatment to prove that heating promotes cross-linking). As shown in Table 1, the samples obtained were labeled as P3S10, P3S5, P5S5, P3S2, and P2S1 (or P3S5K3, P3S5K4, P3S5K5, P3S5K6.5, P3S5K8 if cross linked). The nomenclature is based on the relative mass of PVA, Sep, and KH-550 in the aerogel sample. The specific preparation of the composite aerogels is shown in Fig. 1.

Characterization

The apparent densities of the aerogels were calculated from $\rho = m/v$ (where ρ is the density, m is the weight, and v is the volume). The porosity was measured by a gravimetric method. The sample size was

Table 1 List of aerogel components

Sample	PVA/Sep (g/g)	Sample	PVA/Sep/KH-550 (g/g/g)
P3S10	0.3	P3S5K3	3/5/3
P3S5	0.6	P3S5K4	3/5/4
P5S5	1	P3S5K5	3/5/5
P3S2	1.5	P3S5K6.5	3/5/6.5
P2S1	2	P3S5K8	3/5/8

https://doi.org/10.1007/s42860-023-00228-6 Published online by Cambridge University Press

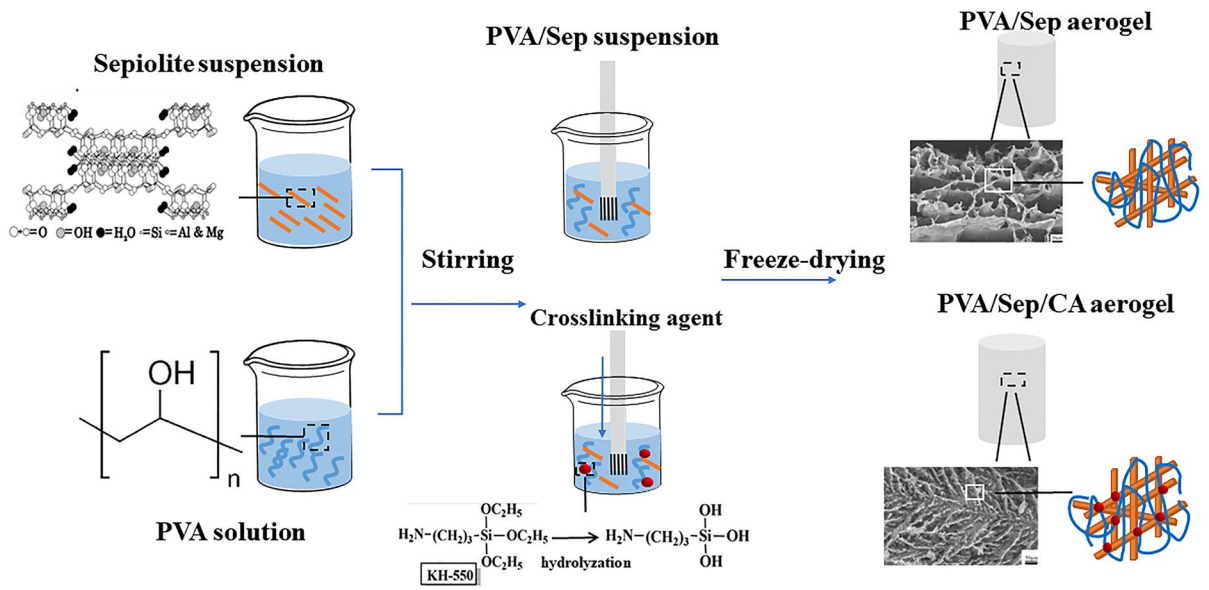

Fig. 1 Preparation process of the composite aerogel

20 mm×20 mm×20 mm and an average value was taken from three measurements. The specific calculation formula was as follows (Sanguanwong et al., 2021b):

$$P = \left(1 - \frac{\rho_a}{\rho_s}\right) \times 100\%$$

$$\rho_s = \frac{1}{\frac{\omega 1}{\rho 1} + \frac{\omega 2}{\rho 2} + \frac{\omega 3}{\rho 3}}$$

$$\rho_a = \frac{m}{V}$$

where P is the porosity; m, mass; V, apparent volume; ρ, density fractions; ρ_a, density of aerogel; ρ_s, skeleton density.

The functional groups of the aerogel composites prepared were analyzed by attenuated total reflectance Fourier-transform infrared spectroscopy (ATR-FTIR, Avatar380, Thermo Fisher Scientific, Waltham, Massachusetts, USA). The spectral analysis range was 400 to 4000 cm^{-1}. The ATR attachment allowed the sample to be placed directly under the test probe without further processing.

The morphology of the aerogel samples was examined by scanning electron microscopy (SEM, TM3030, Hitachi Co., Ltd., Tokyo, Japan) at an acceleration voltage of 15 kV. In the sample-preparation process, the aerogel was first frozen in liquid nitrogen and then sliced with a blade to obtain a cross section. The cross section of the sample was then stuck on the section observation platform and observed after spraying with gold.

The crystal structure of the aerogel samples was analyzed by X-ray diffraction (XRD D/max 2550PC, Rigaku, Tokyo, Japan). The aerogel samples were taped flat on a glass plate, stuck into the sample slot, and scanned in the test range 5–90°2θ.

The elements of the aerogel samples were analyzed by X-ray photoelectron spectroscopy (XPS Escalab 250Xi, Yuzhong Industrial Co., Ltd, Shanghai, China). The sample size was 3 mm×3 mm×3 mm.

The thermal conductivity of aerogels was measured using the transient planar heat source method (Hot Disk TPS 2500S, Gothenburg, Sweden) at room temperature (25°C). The sample size was 50 mm×50 mm×10 mm.

Aerogel composites were tested using a BS EN ISO 604 universal testing machine (HY 940F, Yuzhong Industrial Co., Ltd, Shanghai, China) at 45% RH and 23°C (this instrument measures the compression properties of an aerogel or the tensile properties of a film and the stress–strain curve can be derived directly after instrument testing, without additional calculation and process). The tester speed was 20 mm/min and the test end-condition was 50% strain. The compression modulus of four specimens was measured and the average value was calculated. The sample size was 20 mm×20 mm×20 mm.

https://doi.org/10.1007/s42860-023-00228-6 Published online by Cambridge University Press

The limiting oxygen index (LOI) values of the samples were tested on an oxygen index instrument (ATS 1,004,050, ATS FAAR S.p.A, Shanghai, China) with the samples at a size of 100 mm × 10 mm × 10 mm.

Thermogravimetric analyses (TG 209F1, Netzsch, Shanghai, China) of the 5 mg samples were done in a nitrogen atmosphere at temperatures ranging from 30 to 900°C at a rate of 10°C/min.

A vertical combustion test for aerogel samples according to the UL-94 experiment was conducted (Wu et al., 2019). The sample size was 125 mm × 10 mm × 10 mm.

The relevant combustion values of the aerogel samples were measured using a microcombustion calorimeter (MCC FAA-PCFC, British Fire and Combustion Characteristics Test Technology Co. Ltd, Manchester, UK) according to the ASTM D7309-2007 standard (Luo et al., 2022). A ~5 mg sample was heated from room temperature to 750°C for pyrolysis at a nitrogen flux of 80 cm^3/min, and the temperature-increase rate was maintained at 1°C/s. The main purpose of this test was to evaluate the flame retardancy of aerogels. In this paper, the flame retardancy of aerogel was characterized by the MCC test.

The excitation wavelength of 532 nm of the Raman spectrometer (DXR2xi, Thermo Fisher Scientific, Waltham, Massachusetts, USA) was used to determine the residual carbon for the aerogel. The aerogel residual carbon was attached directly to the slide for testing without further processing.

Results and Discussion

Optimization of Preparation Conditions

The Effect of pH on Sep Suspension Stability

The surface charge of Sep was sensitive to pH, which directly affected the three-dimensional arrangement of the Sep skeleton structure in the aqueous dispersion (Baldermann et al., 2018). Therefore, controlling the pH of the Sep dispersion environment was necessary.

Sep was dispersed in a series of aqueous solutions with varying pH values that were adjusted by using 0.1 mol/L hydrochloric acid or 0.1 mol/L sodium hydroxide solution to obtain Sep suspensions. The stratification of Sep suspensions after 24 h is shown in Fig. 2, the viscosity of the Sep suspensions was measured, as shown in Table 2. The viscosity of Sep suspensions in an acidic environment was obviously greater than in an alkaline environment. In an ideal state or model, Mg^{2+} will occupy each octahedral position of Sep, but in the actual environment, Mg^{2+} and Si^{4+} in Sep tetrahedra will be replaced, resulting in the generation of negative charges and structural changes. Therefore, the surface charge of Sep is very sensitive to pH, and it is easy to precipitate in an alkaline environment (Wu et al., 2022). At a pH value of 4.62, the viscosity of the Sep suspension peaked at 1.08 Pa s. After 24 h of resting, Sep suspensions in the alkaline environment revealed an obvious delamination (Fig. 2b). Evident solid precipitation appeared at the bottom of the alkaline suspensions in the inverted glass bottle, and the delamination of Sep intensified as the alkalinity of the suspensions increased. In addition, after 24 h of resting in a neutral or acidic environment, the fluidity of suspensions decreased significantly. This was due to the fact that the structure of the Sep sol–gel network in neutral or acid environments is more stable, whereas the Sep sol–gel network could not form in an alkaline environment (Baldermann et al., 2018). Therefore, a pH value of 4.62 was selected to prepare Sep suspensions for subsequent experiments.

The Effect of PVA/Sep Mass Ratio on Aerogel Properties

The addition of PVA can help to improve the mechanical properties of Sep-based aerogels. A series of aerogels was produced by controlling the PVA/Sep mass ratio, and the physical parameters of the aerogels are shown in Table 3. The density of the prepared aerogels was < 0.5 g/cm^3 and the porosity was > 96%. With increasing addition of PVA, the density of aerogel increased, the porosity decreased, the compressive modulus decreased from 240.08 to 134.56 kPa, and the resilience increased to 93.51% after a 50% compressive deformation. This was due to the fact that the addition of PVA results in the formation of hydrogen bonding between C–OH in the structure of PVA and Si–OH on the surface of Sep, which can improve the resilience of the Sep-aerogel. With the increase in the amount of PVA added, the PVA within the system underwent a self-cross-linking reaction, and a local

https://doi.org/10.1007/s42860-023-00228-6 Published online by Cambridge University Press

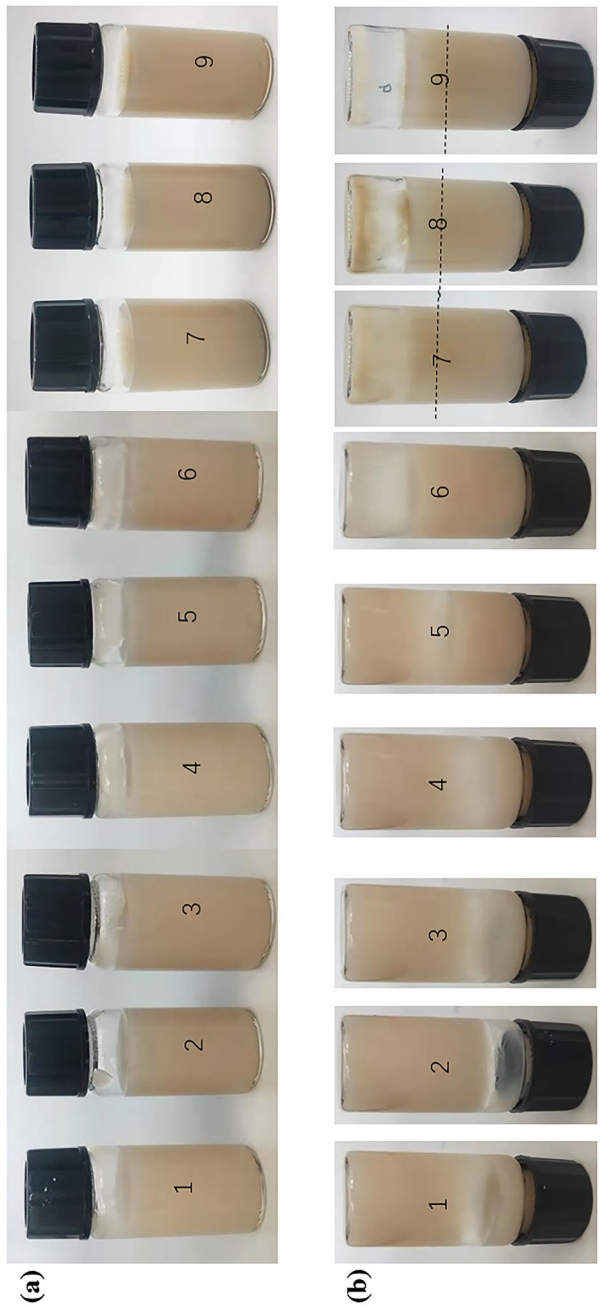

Fig. 2 Stability of Sep suspensions under various pH conditions: **a** glass bottles upright after 24 h of resting; **b** glass bottles inverted from **a** group upright bottles immediately

https://doi.org/10.1007/s42860-023-00228-6 Published online by Cambridge University Press

Table 2 Table of viscosity values of 3 wt.% Sep dispersions at various pH conditions

Sample	1	2	3	4	5	6	7	8	9
pH	3.58	4.62	5.65	6.09	7.15	8.84	9.20	10.83	11.33
Viscosity (Pa s)	1.00	1.08	1.01	0.94	0.76	0.69	0.01	0.005	0.004

Table 3 Basic parameters of PVA/Sep aerogel

Sample	Density (g/cm^3)	Porosity (%)	Modulus (kPa)	Specific Modulus ($MPa{\cdot}cm^3/g$)	R[a] (%)
P3S10	0.0275	98.44	240.08	8.73	85.22
P3S5	0.0281	98.28	209.28	7.45	90.70
P5S5	0.0294	98.18	171.66	5.84	92.43
P3S2	0.0303	98.01	142.14	4.69	93.99
P2S1	0.0308	97.86	134.56	4.37	93.51

[a] $R = \frac{H2-H1}{H0-H1} \times 100$ = Extent of rebound after 50% compression, where H_0 is the original height of the sample (mm); H_1, height after compression to 50% (mm); H_2, rebound height at 60 s after removal of external force (mm) (Guo et al., 2018)

Table 4 Basic parameters of crosslinked aerogels

Sample	Density (g/cm^3)	Porosity (%)	Modulus (kPa)	Specific Modulus ($MPa{\cdot}cm^3/g$)	R[a] (%)
P3S5K3	0.0372	97.25	341.50	9.18	86.21
P3S5K4	0.0376	97.15	350.87	9.33	87.89
P3S5K5	0.0428	96.65	474.43	11.08	89.31
P3S5K6.5	0.0441	96.38	373.32	9.08	86.80
P3S5K8	0.0477	96.09	259.92	5.45	85.13

[a]See footnote to Table 3

agglomeration phenomenon occurred in Sep, thus reducing the mechanical properties. The compression modulus of P3S5 was 209.28 kPa (Table 3), and the resilience reached 90.70%, which was the best physical performance overall. For this reason, the mass ratio for PVA/Sep selected in subsequent experiments was 0.6.

The Effect of the Mass of Cross-Linking Agent on Aerogel Properties

In sample P3S5, the Si–OH on the surface of Sep and the C–OH in the structure of PVA were bound by hydrogen bonds. To improve the mechanical properties of the Sep-based aerogels further, the addition of the cross-linking agent KH-550 was chosen to enable the formation of chemical cross-linking (Si–OH of KH-550 and C–OH of PVA; Si–OH of KH-550 and Si–OH of Sep) and hydrogen bonding (–NH_2 of KH-550 and –OH of PVA; –NH_2 of KH-550 and –OH of Sep; –OH of PVA and –OH of Sep) (Cao et al., 2018; Guo et al., 2006; Zhao et al., 2022). By varying the amount of KH-550, a range of cross-linked aerogels was created, and the exact physical characteristics are given in Table 4. The density of the prepared aerogels was < 0.5 g/cm^3 and the porosity was > 96%. The compression modulus increased at first and then decreased, rising from 341.50 to 474.43 kPa and then falling to 259.92 kPa as a result of the addition of excessive cross-linking agent, which caused excessive Sep agglomeration, affecting the mechanical properties of the crosslinked aerogels. By combining the data above, the P3S5K5 sample was finally selected for the subsequent testing and characterization.

Structural and Morphological Aspects of Aerogels

The compositions of the aerogels were investigated using FTIR and XPS (Fig. 3). The FTIR band at 3325 cm^{-1} was ascribed to –OH of PVA. The band at 1008 cm^{-1} was ascribed to Si–O–Si of Sep. The hydroxyl stretching vibration band of P3S5 at 3325 cm^{-1} became wider and weaker, while the Si–O–Si vibrational peak at 1000 cm^{-1} shifted slightly to the lower wavenumber, indicating the formation of hydrogen bonds between PVA and Sep (Madyan & Fan, 2017; Pang et al., 2021; Simon-Herrero et al., 2019). In contrast, the FTIR of P3S5K5 showed characteristic absorption peaks of –NH_2 at 1535 cm^{-1}, and Si–O–C and Si–O–Si at 1146 and 1008 cm^{-1}, respectively (Sanguanwong et al., 2021a; Turhan et al., 2008; Xie et al., 2010). When compared to pure PVA aerogel, the stretching vibration peak of the hydroxyl group at 3325 cm^{-1} widened and weakened, and a new absorption peak from Si–O–C appeared (Zhu et al., 2022), indicating that the –OH in the structure

https://doi.org/10.1007/s42860-023-00228-6 Published online by Cambridge University Press

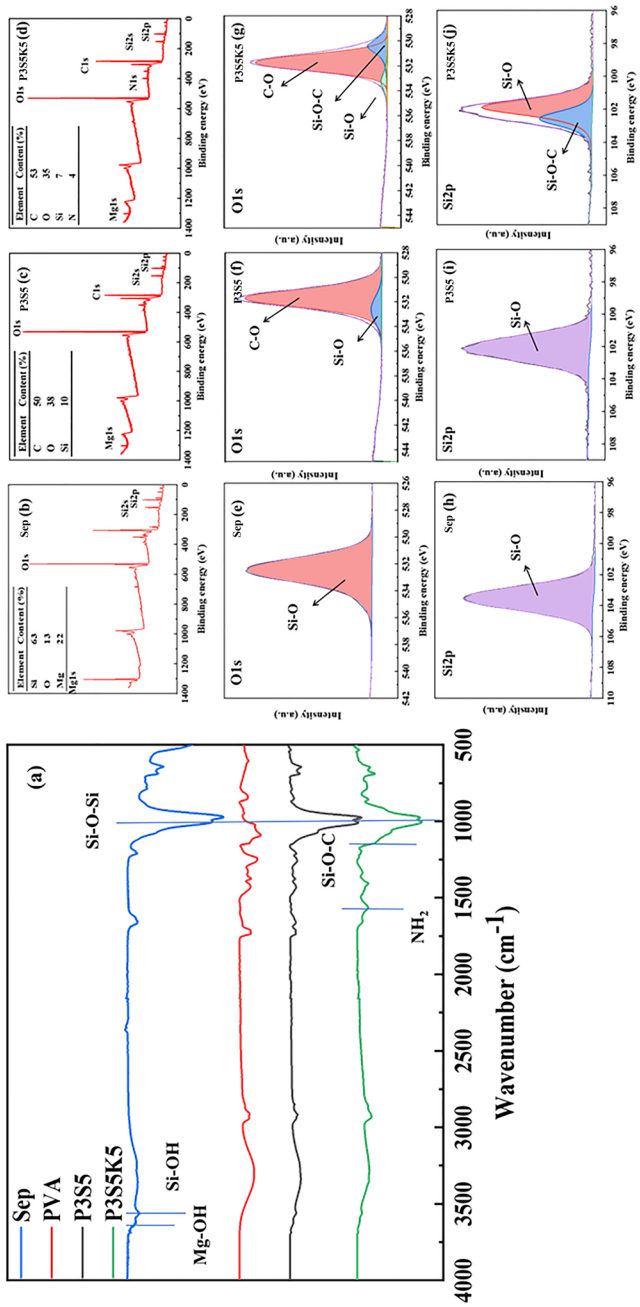

Fig. 3 **a** FTIR spectra of Sep, PVA, and composite aerogels. XPS of aerogels: **b**,**e**,**h** Sep; **c**,**f**,**i** P3S5; **d**,**g**,**j** P3S5K5

https://doi.org/10.1007/s42860-023-00228-6 Published online by Cambridge University Press

of PVA formed a chemical cross-link with the Si–OH of KH-550 (Fig. 3a).

The XPS spectra (Fig. 3b–j) revealed that the elemental content fluctuation in the composites was visible across the entire spectrum, and the aerogel contained N atoms after the cross-linking agent was added (the N element was derived only from KH-550, the crosslinking agent). The O1s peak for Sep (Fig. 3e) corresponded only to Si–O (532.5 eV) (Qiu et al., 2019). In P3S5, the O1s peak was deconvoluted into two peaks (Fig. 3f), one for C–O (531.7 eV) and one for Si–O (532.7 eV). The position of the Si–O peak shifted slightly to lower energy. Deconvolution of the O1s peak from sample P3S5K5 (Fig. 3g) had three peaks which meant that oxygen has three forms of bonding, corresponding to C–O (531.9 eV), Si–O (533.3 eV), and Si–O–C (530.5 eV) (Zhu et al., 2022). Additional analysis of the Si2p peaks found that the position of the Si–O peak in the P3S5 sample was shifted significantly to lower energy relative to Sep, from 103.5 eV to 102.1 eV. (Fig. 3h–i). This could indicate that the Si–OH on the surface of Sep formed hydrogen bonds with the C–OH of PVA. In P3S5K5, a new peak corresponding to Si–O–C (102.9 eV) appeared, which could effectively prove that Si–OH in KH-550 and C–OH in PVA could be cross-linked chemically to form Si–O–C after the addition of KH-550 (Fig. 3j) (Jiang et al., 2019).

The crystalline structures of the samples were studied by XRD (Fig. 4a), which produced a strong diffraction peak in sample Sep at 7.38°2θ, corresponding to the crystallographic diffraction of Sep (110). PVA exhibited a strong diffraction peak at 22.71°2θ, corresponding to its (200) crystallographic plane. In the XRD pattern of the P3S5 sample, the position of the strong diffraction peak belonging to Sep did not change, and thus the layer spacing was unchanged at ~1.19 nm, indicating that the PVA molecular chain did not intercalate into the Sep interlayer. Because Sep is different from montmorillonite and has no lamellar structure, intercalation did not occur in the composite (Huang et al., 2012). In addition, the peaks of Sep and PVA were still present in the diffraction pattern of P3S5, no new peaks appeared, and peak positions did not change significantly, indicating that the addition of PVA did not affect the crystal structure of Sep. In the P3S5K5 composite aerogel, the strong diffraction peak belonging to Sep moved from 7.38 to 7.79°2θ. According to the Bragg equation, $2d\sin\theta = n\lambda$, the layer spacing decreased from 1.19 to 1.13 nm, caused by the addition of KH-550 which broke the covalent bond between the Sep lamellae (Aslam et al., 2018; Lu et al., 2004).

As shown in Fig. 4b, aerogels of different shapes and sizes had been fabricated as required. The cross sections of the aerogels (Fig. 4d–h) showed a distinct 3D mesh structure in the P3S5 aerogel, and greater magnification revealed a distinct fibrous entanglement structure in the cell wall (Fig. 4e); this was the skeletal structure formed by Sep (Farooq et al., 2018). Compared with P3S5, the addition of a cross-linking agent made the 3D porous structure of the material more compact, which was due to the presence of both physical and chemical cross-linking forces between the components of the system, and the magnification of the scan also showed the skeletal structure formed by Sep (Fig. 4f).

Thermal Conductivity and Combustion Performance of Aerogel

Thermal conductivity was an important parameter for evaluating the thermal insulation properties of the material (Table 5). The thermal conductivity of the P3S5 sample was 0.0328 W/(m K), less than reported elsewhere (Table 6) (Di et al., 2022; Guo et al., 2022; Gupta et al., 2019; Li et al., 2022; Madyan & Fan, 2018; Sun et al., 2021; Wang et al., 2020; Zhao et al., 2021). The LOI of the P3S5 sample was 26.4% and increased to 30.4% with the addition of the cross-linker KH-550. The results of the vertical combustion test on two samples (Fig. 5c) showed that, after contact with the flame, a black charcoal layer formed on the surface of the aerogel immediately, which self-extinguished immediately after removal of the flame and could not be re-ignited. According to the UL-94 standard rating, P3S5 and P3S5K5 could reach a flame retardancy level of V-0 (according to the ASTMD3801-10 standard, the V-0 grade is achieved when the burning time of two consecutive combustions is within 10 s with no droplet generation; this test can show that the aerogel sample has good flame retardancy). After vertical combustion, the damage length (the maximum length, expressed in centimeters, of the damaged part of the material in the vertical direction under specified test conditions) of the P3S5K5 sample was shorter than that of the P3S5

https://doi.org/10.1007/s42860-023-00228-6 Published online by Cambridge University Press

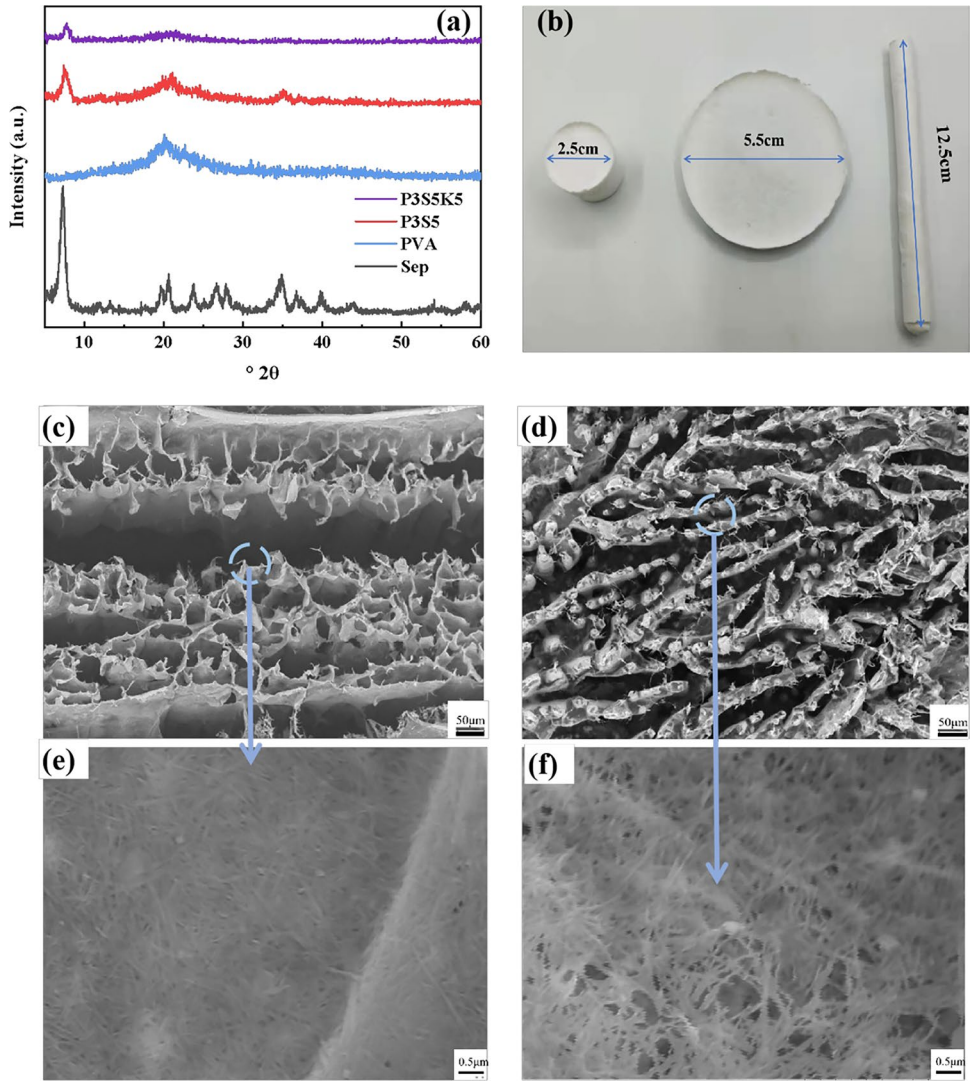

Fig. 4 **a** XRD of aerogels; **b** photos of various sizes of sample P3S5; SEM images of aerogels: **c,e** P3S5, **d,f** P3S5K5

Table 5 Thermal conductivity, compostion properties, and thermal-stability parameters of aerogels

Sample	Thermal conductivity (W/(m·K))	LOI (%)	UL-94	$T_{d10\%}$ (℃)	T_{dmax} (℃)	d*W*/d*T* (%/℃)	Residue (%)
P3S5	0.0328	26.4	V-0	248.6	294.0	4.20	44.8
P3S5K5	0.0390	30.4	V-0	242.6	249.0	3.35	54.9

sample, and the cross-linking agent also increased the flame retardancy of the Sep-based aerogel.

The thermal stability of the Sep-based aerogels was investigated by thermogravimetric analysis in nitrogen (Table 5, Fig. 5). The mass loss of the aerogels at ~100°C reflected the removal of adsorbed water (Fig. 5a,b). Compared with P3S5 (taking P3S5 as the standard), the initial decomposition

https://doi.org/10.1007/s42860-023-00228-6 Published online by Cambridge University Press

Table 6 Thermal conductivity of aerogels

Aerogel	Thermal conductivity (W/(m·K))	References
P3S5	0.0328	This work
P3S5K5	0.0390	This work
Montmorillonite/PVA/PA aerogel	0.0563	Wang et al. (2020)
Tubular cellulose/montmorillonite Aerogel	0.0540	Sun et al. (2021)
Montmorillonite/PVA/WDisRep1 aerogel	0.0430	Madyan & Fan (2018)
Cellulose/sepiolite/glutaraldehyde aerogel	0.0396	Pragya Gupta et al. (2019)
PVA/graphene/nanocellulose aerogel	0.050	Wang et al. (2021)
Laponite®/silicone aerogel	0.0360–0.0480	Li et al. (2022)
Agar/PVA/Palygorskite/Magnesium hydroxide aerogel	0.0423–0.0454	Guo et al. (2022)
SiO_2/KH-550 aerogel	0.050	Di et al. (2022)

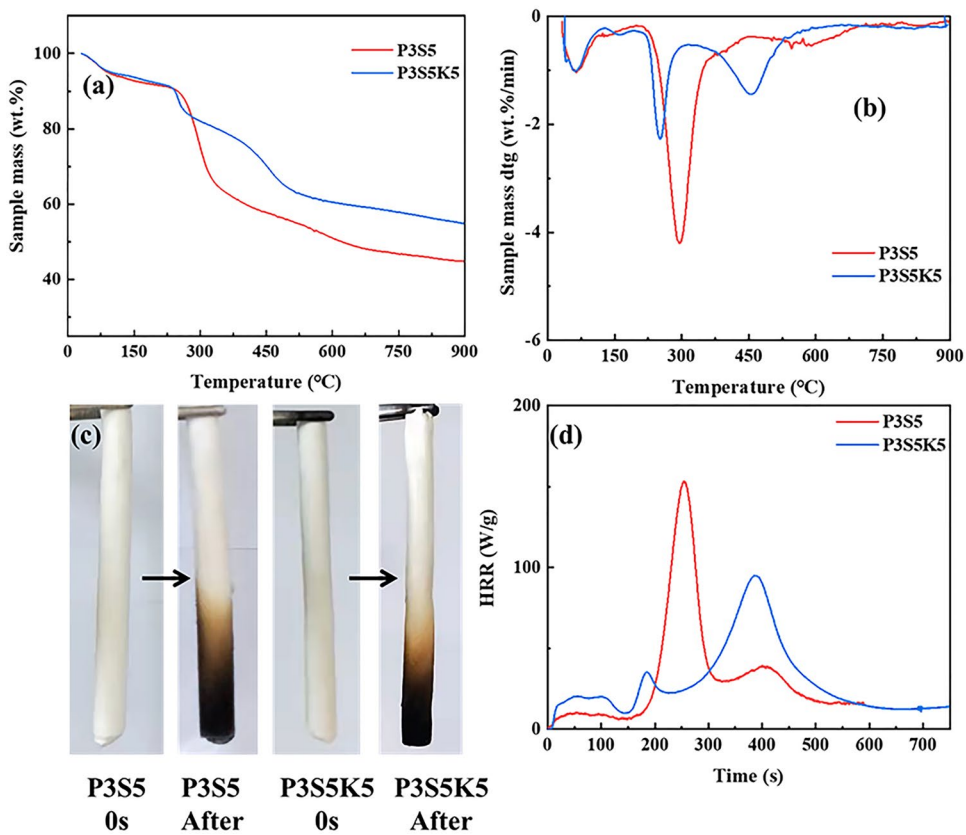

Fig. 5 High-temperature resistance of aerogels: **a** TG; **b** DTG; **c** aerogels before and after vertical burning tests; **d** heat-release rate (HRR) temperature curves

https://doi.org/10.1007/s42860-023-00228-6 Published online by Cambridge University Press

temperature of P3S5K5 decreased to 242.6°C, the maximum decomposition temperature was reduced by 48°C, and the residual carbon content increased significantly to 54.9% at 900°C. This indicated that the addition of KH-550 accelerated the initial decomposition of Sep-based aerogel in the flame and the formation of surface coke, and that the coke layer prevented the aerogel from further decomposition by oxidation.

To evaluate the combustion performance of aerogels further, the heat-release rate (HRR), total heat release (THR), heat-release capacity (HRC), and the peak of heat release rate (pHRR) of aerogels were measured using a microcalorimeter (Table 7, Fig. 5d). The HRR is the most important parameter for characterizing the combustion performance of materials and is the primary basis for evaluating the fire risk of materials. After adding the KH-550, the heat-release capacity of the aerogel was reduced from 141 to 137 J/(g k), the pHRR was reduced from 152.9 to 95 W/g, a reduction of 37.9%, and the temperature of pHRR increased from 314.5 to 386.9°C. These data indicated that the addition of KH-550 improves the flame retardancy of the Sep-based aerogel.

Analysis of the Flame-Retardant Mechanism

The residues of P3S5 and P3S5K5 from the vertical combustion tests were investigated by means of SEM imaging and FTIR spectroscopy (Fig. 6) to assess the changes in the morphology and porous structure and the chemical composition after burning. The initial porous structure of P3S5 and P3S5K5 was preserved in the same way as the structure of the samples without combustion (Fig. 6a,d). When the materials were observed under magnification, they showed fibrous structures in the cell walls, indicating that the skeletal support provided by Sep during burning was important in maintaining the aerogel structure (Fig. 6b,e).

Table 7 Microcombustion calorimeter test results of aerogels[a]

Sample	HRC (J/(g·k))	pHRR (W/g)	THR (kJ/g)	T_{max} (°C)
P3S5	141	152.9	10.9	314.5
P3S5K5	137	95.0	8.8	386.9

[a]HRC: heat-release capacity; pHRR: peak of heat release rate; THR: total heat release

FTIR analysis was used to measure changes in bond vibrational energies in the residues (Fig. 6c). While the Si–O–Si absorption peak was retained at 1008 cm^{-1}, the burned samples P3S5 and P3S5K5 showed bands of C=C stretching and C–H bending vibrations at 1650 and 790 cm^{-1}, respectively, with no aliphatic absorption between 2800 and 3000 cm^{-1}. This indicated that a conjugated aromatic carbonaceous structure was formed during combustion (Ghanadpour et al., 2018). This was consistent with the formation of thermally stabilized carbon in the samples. In the P3S5K5, the Si–O–C at 1146 cm^{-1} was retained after combustion, indicating that the addition of KH-550 prevented effectively the combustion within the aerogel. In addition, Sep could promote the rapid dehydration of the aerogel surface into carbon and inhibit strong blistering during combustion degradation, resulting in flame-retardant protection (Gupta et al., 2019; Jiang et al., 2019).

In the characterization of flame-retardant materials, Raman spectroscopy was also used to understand the nature of the residual carbon obtained after the combustion of the material, so that the flame retardant mechanism could be better understood. Raman spectroscopy was performed on the residual carbon of P3S5 and P3S5K5 samples, and the resulting spectra (Fig. 6f) revealed two distinct peaks of the aerogel, corresponding to the D and G peaks of the C atom, respectively. The D band at 1362 cm^{-1} represented the amorphous carbon and lattice defects, while the G band at 1596 cm^{-1} represented the in-plane stretching vibration of the Sp2 hybridization of the C atom. The peak intensity ratio R (ID/IG) of the two bands of D and G reflected the degree of graphitization of the carbon material tested; the lower the R value, the greater the degree of graphitization of the carbon material, which meant that the carbon-forming performance of the corresponding material was better (Kang et al., 2019). The R-values for P3S5 and P3S5K5 were 1.6 and 1.2, respectively, for which both are considered to be low levels. Furthermore, P3S5K5 had better carbon-formation performance than P3S5, and the addition of a cross-linking agent improved the flame retardant performance of the aerogel.

Mechanical Properties of Aerogels

Excellent mechanical properties are the basis for application in tents. The mechanical properties of

https://doi.org/10.1007/s42860-023-00228-6 Published online by Cambridge University Press

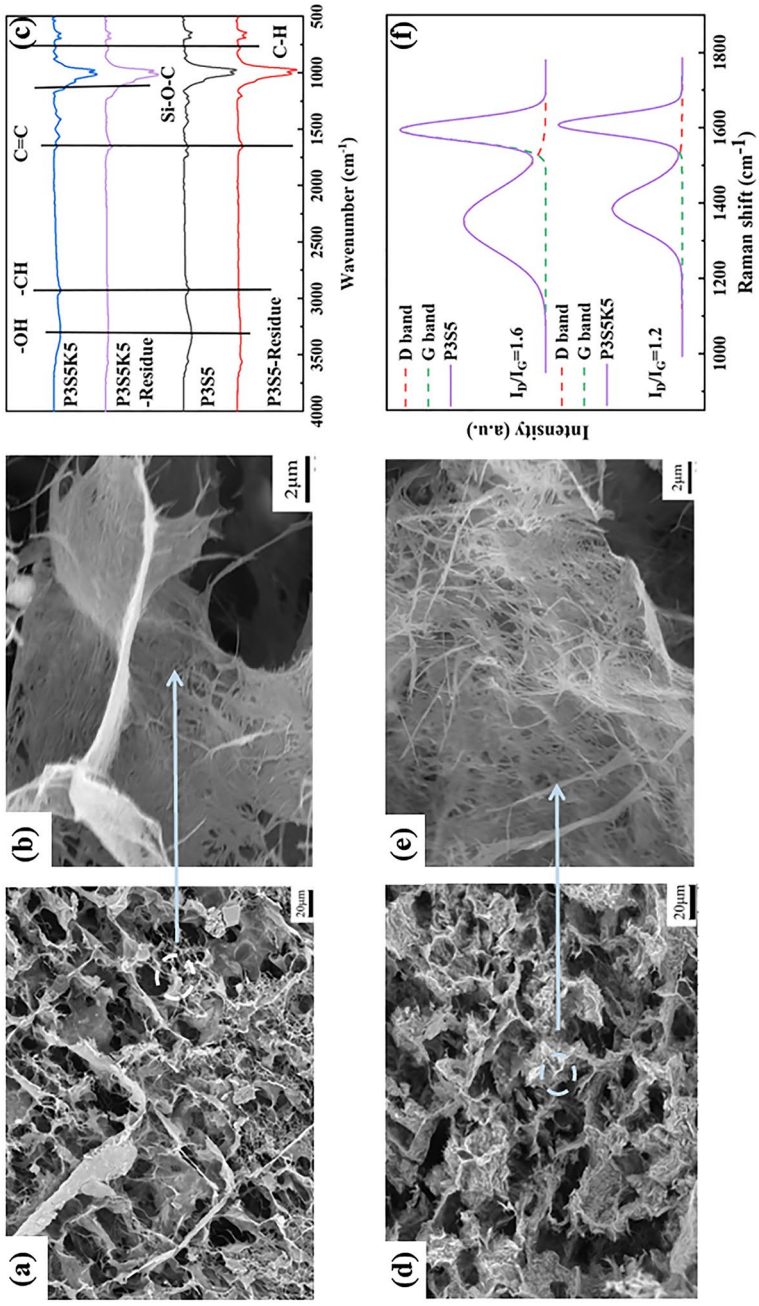

Fig. 6 SEM and FTIR images of aerogel residue: **a,b** P3S5 and **d,e** P3S5K5; **c** FTIR spectra of residue; **f** Raman spectra of the carbon layer of residue

https://doi.org/10.1007/s42860-023-00228-6 Published online by Cambridge University Press

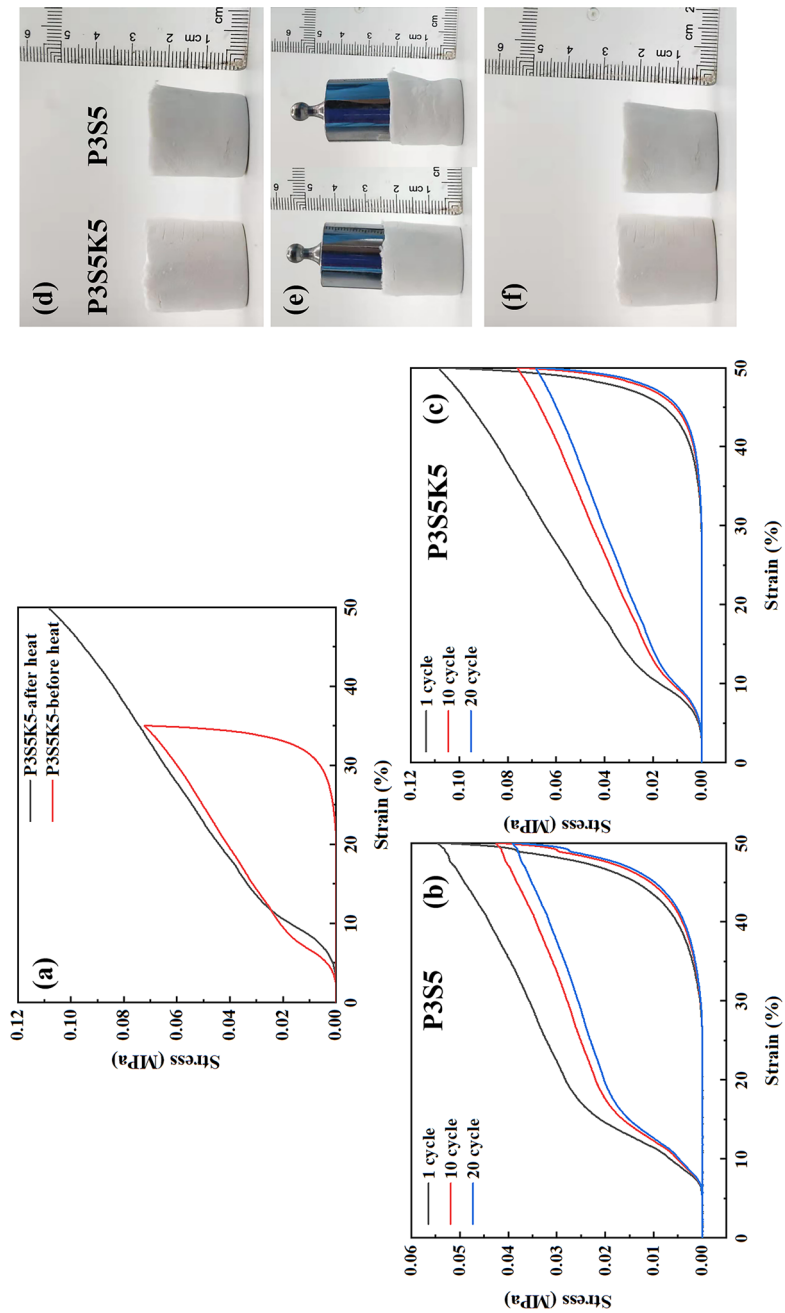

Fig.7 **a** Stress–strain curves for sample P3S5K5 before and after heat treatment to 110ºC for 30ºmin; stress–strain cycle curves for samples **b** P3S5 and **c** P3S5K5; images of samples P3S5K5 and P3S5 **d** before the compressive force was applied, **e** at the point at which the compressive force was applied, and **f** 60 s after the compressive force was removed

https://doi.org/10.1007/s42860-023-00228-6 Published online by Cambridge University Press

aerogels would be affected by the addition of PVA, cross-linking agents, and cross-linking between the aerogel components. The density of the Sep-based aerogels was < 0.5 g/cm^3 and the porosity was > 96%. The compressive modulus of the P3S5 sample was 209.28 kPa. The modulus of P3S5K5 increased to 474.43 kPa, which was 2.6 times its original value, following the addition of the cross-linking agent. In addition, the specific modulus increased to 11.08 MPa cm^3/g and, after compression to 50% deformation, it reached 89.31% resilience. The stress–strain cycle curves of aerogels (Fig. 7b,c) showed that, in the initial stage of compression, the sample exhibited linear elastic properties, which determined the compression modulus. The stress–strain curve was smooth throughout the test phase with no sudden drop, indicating that the aerogel did not break during the compression process.

The loading and unloading cycles of P3S5 and P3S5K5 under 50% axial strain were used to study the elastic properties of the materials. The compression property of sample P3S5K5 was obviously improved after heating, which was caused by the cross-linking promoted by heating (Fig. 7a). After 20 cycles, the two samples showed typical hysteresis loop curves, but still maintained good resilience, indicating that the composite aerogel has good fatigue resistance and long-term stability (Fig. 7b,c). The rigidity of P3S5K5 was better than that of P3S5. P3S5K5 was able to support a 50 g weight without deformation when the 50 g weight was applied to the aerogel, whereas P3S5 showed slight deformation under the pressure generated by the 50 g weight (Fig. 7d). When the P3S5K5 and P3S5 were compared before and after applying pressure (Fig. 7e,f), no significant changes were noted and no cracks appeared.

Conclusion

In summary, a simple and environmentally friendly freeze-drying technology was used to prepare thermal-insulation and flame-retardant composite aerogels. By studying the mass ratio of PVA and Sep, the aerogels with low density (0.0275–0.0308 g/cm^3), low thermal conductivity (0.0309–0.0438 W/m·K), high compression resilience, and excellent flame-retardant performances were obtained. With the addition of cross-linking agent KH-550, the mechanical strength of aerogels was improved significantly (the compression modulus reached 474.443 kPa), and the flame-retardant performance was further increased (LOI index reached 30.4%). This was because the addition of KH-550 made chemical cross-linking (Si–OH of KH-550 and C–OH of PVA; Si–OH of KH-550 and Si–OH of Sep) and hydrogen bonding (–NH_2 of KH-550 and –OH of PVA; –NH_2 of KH-550 and –OH of Sep; –OH of PVA and –OH of Sep) formed inside the system, thus improving the mechanical and thermal properties of the composite aerogel. The results show that the thermal insulation and flame-retardant composite aerogels made of low-cost and environmentally friendly materials are feasible and promising in terms of possible use as an interlayer in an outdoor tent.

Acknowledgements This work was supported financially by the Fundamental Research Funds for the Central Universities No. 2232022G-04 and the International Cooperation Fund of Science and Technology Commission of Shanghai Municipality (No. 21130750100)

Funding Fundamental Research Funds for the Central Universities No. 2232022G-04 and the International Cooperation Fund of Science and Technology Commission of Shanghai Municipality (No. 21130750100).

Data Availability All data generated or analysed during this study are included in the manuscript.

Declarations

Ethics Approval and Consent N/A

Consent for Publication N/A

Competing Interests The authors declare that they have no conflicts of interest.

References

Alkan, M., Tekin, G., & Namli, H. (2005). FTIR and zeta potential measurements of sepiolite treated with some organosilanes. *Microporous and Mesoporous Materials, 84*, 75–83.

Aslam, M., Kalyar, M. A., & Raza, Z. A. (2018). Polyvinyl alcohol: A review of research status and use of polyvinyl alcohol based nanocomposites. *Polymer Engineering and Science, 58*, 2119–2132.

Baldermann, A., Mavromatis, V., Frick, P. M., & Dietzel, M. (2018). Effect of aqueous si/mg ratio and ph on the

https://doi.org/10.1007/s42860-023-00228-6 Published online by Cambridge University Press

nucleation and growth of sepiolite at 25 degrees C. *Geochimica et Cosmochimica Acta, 227*, 211–226.

Cao, M., Wang, C., Xia, R., Chen, P., Miao, J., Yang, B., Qian, J., & Tang, Y. (2018). Preparation and performance of the modified high-strength/high-modulus polyvinyl alcohol fiber/polyurethane grouting materials. *Construction and Building Materials, 168*, 482–489.

Chen, H.-B., Chiou, B.-S., Wang, Y.-Z., & Schiraldi, D. A. (2013). Biodegradable pectin/clay aerogels. *ACS Applied Materials & Interfaces, 5*, 1715–1721.

Cheng, H., Li, Y., Wang, B., Mao, Z., Xu, H., Zhang, L., Zhong, Y., & Sui, X. (2018). Chemical crosslinking reinforced flexible cellulose nanofiber-supported cryogel. *Cellulose, 25*, 573–582.

Di, Z., Ma, S., Wang, H., Guan, Z., Lian, B., Qiu, Y., & Jiang, Y. (2022). Modulation of thermal insulation and mechanical property of silica aerogel thermal insulation coatings. *Coatings, 12*, 1421.

Farooq, M., Sipponen, M. H., Seppala, A., & Osterberg, M. (2018). Eco-friendly flame-retardant cellulose nanofibril aerogels by incorporating sodium bicarbonate. *ACS Applied Materials & Interfaces, 10*, 27407–27415.

Fernandez-Barranco, C., Koziol, A. E., Skrzypiec, K., Rawski, M., Drewniak, M., & Yebra-Rodriguez, A. (2016). Reprint of study of spatial distribution of sepiolite in sepiolite/polyamide6,6 nanocomposites. *Applied Clay Science, 130*, 50–54.

Ghanadpour, M., Wicklein, B., Carosio, F., & Wagberg, L. (2018). All-natural and highly flame-resistant freeze-cast foams based on phosphorylated cellulose nanofibrils. *Nanoscale, 10*, 4085–4095.

Guo, R., Hu, C., Pan, F., Wu, H., & Jiang, Z. (2006). PVA-GPTMS/TEOS hybrid pervaporation membrane for dehydration of ethylene glycol aqueous solution. *Journal of Membrane Science, 281*, 454–462.

Guo, L. M., Chen, Z. L., Lv, S. Y., & Wang, S. Q. (2018). Structure and properties of BTCA cross-linked nanocellulose aerogels. *Forestry Science, 54*, 113–120.

Guo, X., Qiang, X., Chen, G., Su, H., Ouyang, C., Chen, S., & Huang, D. (2022). Facile construction of flame-retardant, heat-insulating agar/polyvinyl alcohol composite aerogels via in situ formation of magnesium hydroxide and palygorskite-assisted strategy. *Journal of Vinyl & Additive Technology, 28*, 502–517.

Gupta, P., Verma, C., & Maji, P. K. (2019). Flame retardant and thermally insulating clay based aerogel facilitated by cellulose nanofibers. *Journal of Supercritical Fluids, 152*, 104537.

Hostler, S. R., Abramson, A. R., Gawryla, M. D., Bandi, S. A., & Schiraldi, D. A. (2009). Thermal conductivity of a clay-based aerogel. *International Journal of Heat and Mass Transfer, 52*, 665–669.

Huang, D., Wang, W., Xu, J., & Wang, A. (2012). Mechanical and water resistance properties of chitosan/poly(vinyl alcohol) films reinforced with attapulgite dispersed by high-pressure homogenization. *Chemical Engineering Journal, 210*, 166–172.

Jiang, P., Zhang, S., Bourbigot, S., Chen, Z., Duquesne, S., & Casetta, M. (2019). Surface grafting of sepiolite with a phosphaphenanthrene derivative and its flame-retardant mechanism on PLA nanocomposites. *Polymer Degradation and Stability, 165*, 68–79.

Johnson, J. R., III., Spikowski, J., & Schiraldi, D. A. (2009). Mineralization of clay/polymer aerogels: A bioinspired approach to composite reinforcement. *ACS Applied Materials & Interfaces, 1*, 1305–1309.

Kang, B.-H., Lu, X., Qu, J.-P., & Yuan, T. (2019). Synergistic effect of hollow glass beads and intumescent flame retardant on improving the fire safety of biodegradable poly (lactic acid). *Polymer Degradation and Stability, 164*, 167–176.

Khan, Z. I., Habib, U., Mohamad, Z. B., Rahmat, A. R. B., & Abdullah, N. A. S. B. (2022). Mechanical and thermal properties of sepiolite strengthened thermoplastic polymer nanocomposites: A comprehensive review. *Alexandria Engineering Journal, 61*, 975–990.

Kistler, S. S. (1931). Coherent expanded aerogels and jellies. *Nature, 127*, 741.

Konuklu, Y., & Ersoy, O. (2016). Preparation and characterization of sepiolite-based phase change material nanocomposites for thermal energy storage. *Applied Thermal Engineering, 107*, 575–582.

Li, X., Wang, Q., Li, H., Ji, H., Sun, X., & He, J. (2013). Effect of sepiolite fiber on the structure and properties of the sepiolite/silica aerogel composite. *Journal of Sol-Gel Science and Technology, 67*, 646–653.

Li, L., Chen, K., & Zhang, J. (2022). Superelastic clay/silicone composite sponges and their applications for oil/water separation and solar interfacial evaporation. *Langmuir, 38*, 1853–1859.

Liu, L., Chen, H., Shiko, E., Fan, X., Zhou, Y., Zhang, G., Luo, X., & Hu, X. (2018). Low-cost DETA impregnation of acid-activated sepiolite for CO_2 capture. *Chemical Engineering Journal, 353*, 940–948.

Liu, K., Zhang, W., Cheng, H., Luo, L., Wang, B., Mao, Z., Sui, X., & Feng, X. (2021). A nature-inspired monolithic integrated cellulose aerogel-based evaporator for efficient solar desalination. *ACS Applied Materials & Interfaces, 13*, 10612–10622.

Lu, H. J., Liang, G. Z., Zhang, B. Y., Chen, X. B., & Ma, X. Y. (2004). Study on high-performance epoxy resin based composite reinforced by organic sepiolite. *China Plastics, 05*, 51–55.

Luo, Z. H., Ning, H. X., Zhou, X. Y., & Yuan, B. H. (2022). Efficient flame-retardant biomass aerogel endowed with graphene oxide interconnected networks for ultrasensitive fire warning. *Materials Letters, 318*, 132277.

Lv, P., Liu, C., & Rao, Z. (2017). Review on clay mineral-based form-stable phase change materials: Preparation, characterization and applications. *Renewable & Sustainable Energy Reviews, 68*, 707–726.

Madyan, O. A., & Fan, M. (2017). Temperature induced nature and behaviour of clay-PVA colloidal suspension and its aerogel composites. *Colloids and Surfaces A-Physicochemical and Engineering Aspects, 529*, 495–502.

Madyan, O. A., & Fan, M. (2018). Hydrophobic clay aerogel composites through the implantation of environmentally friendly water-repellent agents. *Macromolecules, 51*, 10113–10120.

Madyan, O. A., & Fan, M. (2019). Organic functionalization of clay aerogel and its composites through in-situ crosslinking. *Applied Clay Science, 168*, 374–381.

Madyan, O. A., Fan, M., Feo, L., & Hui, D. (2016). Enhancing mechanical properties of clay aerogel composites: An overview. *Composites Part B-Engineering, 98*, 314–329.

Pang, Y., Yu, Z., Chen, L., & Chen, H. (2021). Superhydrophobic polyurethane sponges modified by sepiolite for efficient oil-water separation. *Colloids and Surfaces A-Physicochemical and Engineering Aspects, 627*, 127175.

Pojanavaraphan, T., Schiraldi, D. A., & Magaraphan, R. (2010). Mechanical, rheological, and swelling behavior of natural rubber/montmorillonite aerogels prepared by freeze-drying. *Applied Clay Science, 50*, 271–279.

Pojanavaraphan, T., Liu, L., Ceylan, D., Okay, O., Magaraphan, R., & Schiraldi, D. A. (2011). Solution cross-linked natural rubber (nr)/clay aerogel composites. *Macromolecules, 44*, 923–931.

Qiu, S., Li, Y., Li, G., Zhang, Z., Li, Y., & Wu, T. (2019). Robust superhydrophobic sepiolite-coated polyurethane sponge for highly efficient and recyclable oil absorption. *ACS Sustainable Chemistry & Engineering, 7*, 5560–5567.

Rytwo, G., Nir, S., Margulies, L., Casal, B., Merino, J., & Ruiz-Hitzky, E. (1998). Adsorption of monovalent organic cations on sepiolite: Experimental results and model calculations. *Clays and Clay Minerals, 46*, 340–348.

Salehi, M. H., Golbaten-Mofrad, H., Jafari, S. H., Goodarzi, V., Entezari, M., Hashemi, M., & Zamanlui, S. (2021). Electrically conductive biocompatible composite aerogel based on nanofibrillated template of bacterial cellulose/polyaniline/nano-clay. *International Journal of Biological Macromolecules, 173*, 467–480.

Sanguanwong, A., Flood, A. E., Ogawa, M., Martin-Sampedro, R., Darder, M., Wicklein, B., Aranda, P., & Ruiz-Hitzky, E. (2021a). Hydrophobic composite foams based on nanocellulose-sepiolite for oil sorption applications. *Journal of Hazardous Materials, 417*, 126068.

Sanguanwong, A., Flood, A. E., Ogawa, M., Martin-Sampedro, R., Darder, M., Wicklein, B., Aranda, P., & Ruiz-Hitzky, E. (2021b). Hydrophobic composite foams based on nanocellulose-sepiolite for oil sorption applications. *Journal of Hazardous Materials, 417*, 106026.

Shen, Q., Ouyang, J., Zhang, Y., & Yang, H. (2017). Lauric acid/modified sepiolite composite as a form-stable phase change material for thermal energy storage. *Applied Clay Science, 146*, 14–22.

Simon-Herrero, C., Peco, N., Romero, A., Valverde, J. L., & Sanchez-Silva, L. (2019). PVA/nanoclay/graphene oxide aerogels with enhanced sound absorption properties. *Applied Acoustics, 156*, 40–45.

Sun, J., Wu, Z., An, B., Ma, C., Xu, L., Zhang, Z., Luo, S., Li, W., & Liu, S. (2021). Thermal-insulating, flame-retardant and mechanically resistant aerogel based on bio-inspired tubular cellulose. *Composites Part B-Engineering, 220*, 108997.

Turhan, Y., Turan, P., Dogan, M., Alkan, M., Namli, H., & Demirbas, O. (2008). Characterization and adsorption properties of chemically modified sepiolite. *Industrial & Engineering Chemistry Research, 47*, 1883–1895.

Wang, H., Cao, M., Zhao, H.-B., Liu, J.-X., Geng, C.-Z., & Wang, Y.-Z. (2020). Double-cross-linked aerogels towards ultrahigh mechanical properties and thermal insulation at extreme environment. *Chemical Engineering Journal, 399*, 125698.

Wang, L., Liang, W., Liu, Y., Wang, Y., Mu, W., Wang, C., Sun, H., Zhu, Z., & Li, A. (2022). Carbonized clay pectin-based aerogel for light-to-heat conversion and energy storage. *Applied Clay Science, 224*, 106524.

Wu, N.-J., Niu, F.-K., Liang, W.-C., & Xia, M.-F. (2019). Highly efficient flame-retardant and low-smoke-toxicity poly(vinylalcohol)/alginate/ montmorillonite composite aerogels by two-step crosslinking strategy. *Carbohydrate Polymers, 221*, 221–230.

Wu, C.-R., Hong, Z.-Q., Zhan, B.-J., Tang, W., Cui, S.-C., & Kou, S.-C. (2022). Effect of acid treatment on the reactivity of natural sepiolite used as a supplementary cementitious material. *Construction and Building Materials, 316*, 125860.

Xie, Y., Hill, C. A. S., Xiao, Z., Militz, H., & Mai, C. (2010). Silane coupling agents used for natural fiber/polymer composites: A review. *Composites Part A-Applied Science and Manufacturing, 41*, 806–819.

Zhao, Y.-W., Tian, M.-Z., & Huang, P. (2021). Starch/clay aerogel reinforced by cellulose nanofibrils for thermal insulation. *Cellulose, 28*, 3505–3513.

Zhao, F., Liu, H., Li, H., Cao, Y., Hua, X., Ge, S., He, Y., Jiang, C., & He, D. (2022). Cogel strategy for the preparation of a "thorn"-like porous halloysite/gelatin composite aerogel with excellent mechanical properties and thermal insulation. *ACS Applied Materials & Interfaces, 14*, 17763–17773.

Zhu, T., Zhao, X., Yi, M., Xu, S., & Wang, Y. (2022). Ternary cross-linked PVA-APTES-ZIF-90 membrane for enhanced ethanol dehydration performance. *Advanced Composites and Hybrid Materials, 5*, 91–103.